

Staging model of the ordered stacking of vacancy layers and phase separation in the layered Na_xCoO_2 ($x \gtrsim 0.71$) single crystals

G. J. Shu¹, F. -T. Huang^{1,2,3}, M. -W. Chu¹, J. -Y. Lin⁴, Patrick A. Lee⁵, and F. C. Chou^{1,6*}

¹Center for Condensed Matter Sciences, National Taiwan University, Taipei 10617, Taiwan

²Taiwan International Graduate Program, Academia Sinica, Taipei 10115, Taiwan

³Department of Chemistry, National Taiwan University, Taipei 10617, Taiwan

⁴Department of Physics, National Jiao-Tong University, HsinChu 30076, Taiwan

⁵Department of Physics, Massachusetts Institute of Technology, Cambridge, MA 02139, USA and

⁶National Synchrotron Radiation Research Center, HsinChu 30076, Taiwan

(Dated: October 26, 2018)

Phase diagram of Na_xCoO_2 ($x \gtrsim 0.71$) has been reinvestigated using electrochemically fine tuned single crystals. Both phase separation and staging phenomena as a result of sodium multi-vacancy cluster ordering have been found. Phase separation phenomenon is observed in the narrow ranges of $0.76 \lesssim x \lesssim 0.82$ and $0.83 \lesssim x \lesssim 0.86$. While $x = 0.820$ shows A-type antiferromagnetic (A-AF) ordering below 22K, $x = 0.833$ is confirmed to have a magnetic ground state of A-AF ordering below $\sim 8\text{K}$ and is only reachable through slow cooling. In addition, $x = 0.859$ is found to be responsible for the highest A-AF transition temperature at about 29K. Staging model based on ordered stacking of multi-vacancy layers is proposed to explain the hysteretic behavior and A-AF correlation length for $x \sim 0.82-0.86$.

PACS numbers: 74.62.Bf, 74.25.Bt, 74.62.Dh, 74.78.Fk

I. INTRODUCTION

Layered material Na_xCoO_2 has a rich electronic and magnetic phase diagram as a function of x , from A-type antiferromagnetic ordering for $x \gtrsim 0.75$, to metal-to-insulator transition for $x \sim 1/2$, and even superconductivity for $x \sim 1/3$ after hydration.¹ Although A-type AF magnetic ordering transition below 22K has been reported in all samples of nominal x from 0.75 to 0.85, the difference among these concentrations has usually been ignored, either due to poorly controlled Na level from melt growth or roughly estimated Na content.^{2,3,4} The high Na vapor loss during high temperature melt growth is well known and the diffusive nature of Na ions at room temperature makes the control of Na content even more difficult,⁵ which can often lead to an inhomogeneous mixture of phases for $x \gtrsim 0.7$. Only until recently, detailed Na ion ordering has been revealed through neutron and synchrotron X-ray diffraction studies on single crystal samples.^{6,7} The newly found evidence of superstructure formed by multi-vacancy clusters in $x \sim 0.71$ and 0.84 introduces an idea of doped holes partial localization, which is able to resolve many intriguing physical phenomena found in this layered system, including the Curie-Weiss behavior of a metallic system, the enhanced thermoelectric power, the novel spin liquid state, the reconstructed Fermi surface, and the origin of A-type AF ordering.^{7,8,9} Recent studies of $x \sim 0.80$ and 0.85 by Schulze *et al.* conclude that Na ordering is highly dependent on the cooling rate, where an additional magnetic ordering below 8K appears only after the sample is slowly cooled through the 300-200K range.¹⁰ However, the real impact of the successive Na rearrangement processes remains to be clarified and the phase diagram must be revisited.

Herein, using results from additionally improved electrochemical techniques, specific heat and high resolution single crystal synchrotron X-ray Laue diffraction, we report detailed magnetic and structural phase diagram in the region of $0.71 \lesssim x \lesssim 0.86$. Structural phase separation phenomenon is found in the two regions of 0.76-0.82 and 0.83-0.86 at room temperature as shown in Fig. 1. While simple hexagonal superstructure of $\sqrt{13}a$ is maintained in all samples with x in the range of 0.82-0.86, the magnetic ground state turns out to be distinctively different. In fact, there are three distinct A-AF transition temperatures of $T_{N1}=22\text{K}$, $T_{N2}=8\text{K}$ and $T_{N3}=29\text{K}$ found in this range, corresponding to a proposed specific multi-vacancy layer stack ordering of well-defined stoichiometry of $x = 0.820$, 0.833, and 0.859 respectively, plus $x=0.763$ that shows a spin glass like behavior below $\sim 3\text{K}$ and with a significantly larger superlattice of $\sqrt{19}a$. In particular, we find $x=0.820$ to be the most stable phase and cooling rate independent, while $x=0.833$ shows a strong cooling rate dependent nature with transitions found near 8K (through slow cooling) and 16K (through fast cooling). These distinctively different A-AF phases found in 0.820, 0.833 and 0.859 can be reasonably constructed by adding different levels of additional Na vacancy to the ideal di-vacancy formed $x=11/13=0.846$ superstructure of $\sqrt{13}a \times \sqrt{13}a \times 3c$.^{7,13} Applying a layered staging model similar to that used in graphite intercalated compounds (GIC),¹¹ for example, T_{N1} phase ($x=0.820$) can be described as a stage-2 compound, i.e., where correct stoichiometry is obtained by introducing two more Na vacancies into the original ideal $\sqrt{13}a \times \sqrt{13}a \times 3c$ super unit cell, and these defects create tri-vacancy layers that are sandwiched between every two di-vacancy layers. On the other hand, T_{N2} phase ($x=0.833$) corresponds to stage-5, i.e., tri-vacancy layers are sandwiched between every five

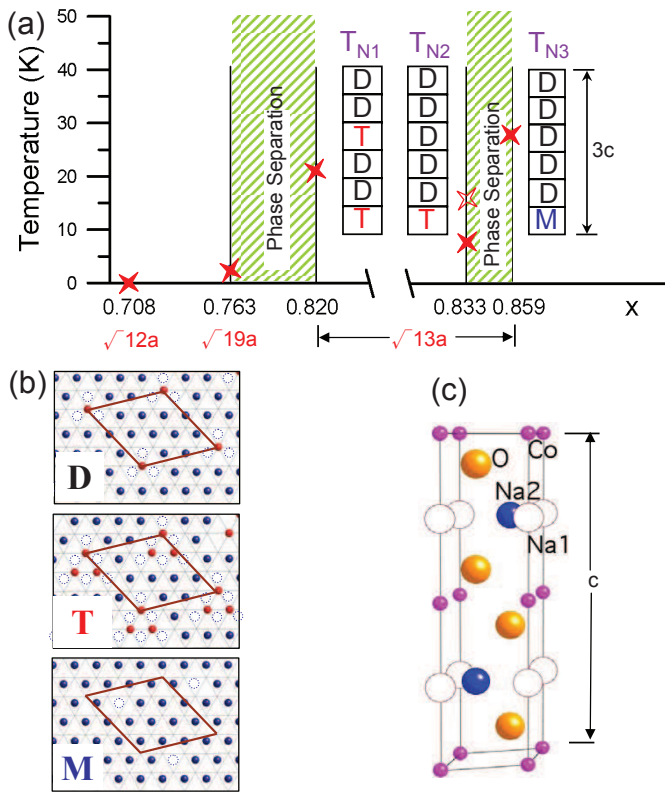


FIG. 1: (color online) (a) A revised phase diagram of Na_xCoO_2 in the range of 0.71-0.86 and the proposed staging models for $x=0.820$ ($T_{N1}=22\text{K}$), 0.833 ($T_{N2}=8\text{K}$) and 0.859 ($T_{N3}=29\text{K}$). Magnetic ordering temperatures are marked by red cross. (b) Na layers with tri-vacancy (T), di-vacancy (D) and mono-vacancy (M), where Na2 ions (blue) move from the original Na2 site (empty circle) to the Na1 site (red). (c) Crystal structure for $\gamma\text{-Na}_x\text{CoO}_2$ of $P6_3/mmc$ symmetry with vacant Na1 sites shown in empty circles.

di-vacancy layers. Most interestingly, the staging model suggests that the trivacancy layers serve as nucleation centers for the interlayer AF ordering. This picture naturally explains why $x=0.820$ has a higher T_N than that of $x=0.833$ because of its shortest inter-trivacancy layer distance. The observed phase separation phenomenon is a natural consequence of the competing multi-vacancy cluster size, superlattice size, and interlayer magnetic correlation.

II. EXPERIMENTAL

High quality single crystals of well controlled Na content were prepared using electrochemical de-intercalation technique starting from high Na content crystal of $x \sim 0.84$ grown with floating-zone method, the details have been documented previously.^{5,7,12} The exact Na content has been cross checked with c-axis vs. x linear relationship constructed from combined high angle

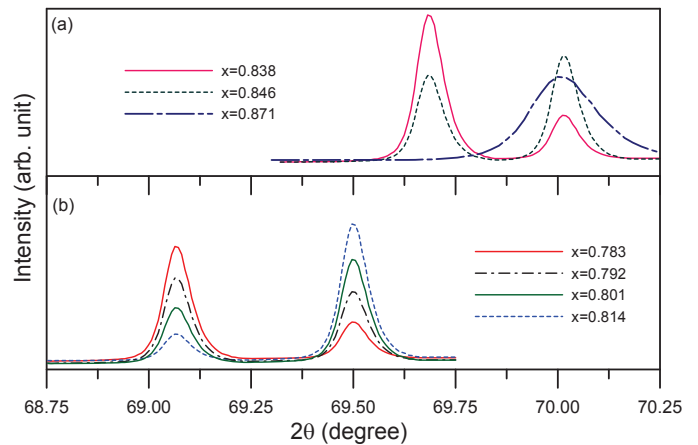


FIG. 2: (color online) (a) X-ray diffraction results of (008) peak for samples with x in the ranges of (a) 0.83-0.87 and (b) 0.76-0.82 at room temperature. The linear x -dependence of relative change of (008) diffraction integrated intensities suggests the phase separation phenomenon. The broadened diffraction peak for $x > 0.86$ as shown in (a) indicates poor ordering.

TABLE I: Summary of studied Na_xCoO_2 crystal samples

sample #	1-5	6-10	11-15	16-20	21-25	
x (EPMA)	0.768(4)	0.801(5)	0.820(3)	0.832(2)	0.842(5)	
x (c-axis)	0.771(2)	PS	0.820(2)	0.832(2)	PS	
x (model)	0.763	PS	0.820	0.833	PS	0.859
T_N (K)*	3**	22	22	8	8/29	

*slow cooling **spin glass like behavior

X-ray diffraction (008) peak position, Inductively Coupled Plasma (ICP) and Electron Probe Microanalysis (EPMA) techniques.^{1,5,7} In particular, current study uses $c(x)$ linear function that is further calibrated by the phase separated boundaries and EPMA is averaged out from freshly cleaved crystal surface for more than 100 points. A complete list of samples studied is summarized in Table I. Due to the active diffusive nature of Na ions at room temperature and the minute differences of Na content, all measurements were done on freshly prepared crystals within days. Otherwise crystal samples must be stored within L-N2 dewar below 200K in order to suppress Na loss from the surface. Synchrotron Laue diffraction for Na superstructure investigation was performed with synchrotron source in Taiwan NSRRC, and magnetic property characterization was done using Quantum Design SQUID MPMS-XL.

III. RESULTS AND DISCUSSIONS

While zooming in the region of $x > 0.75$ using electrochemical technique, we found several concentrations to be particularly stable and of two-phase character. As indicated in Fig. 2, the evidence of phase separation

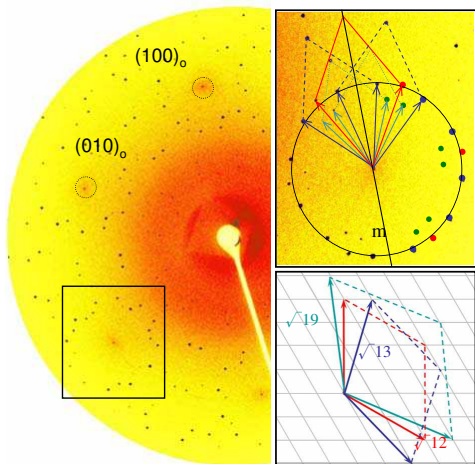


FIG. 3: (color online) Synchrotron X-ray Laue pattern for $x=0.801(5)$ at room temperature, where three twin sets of hexagonal units are shown in the reciprocal space (upper inset), which correspond to hexagonal $\sqrt{13}a$ (blue), $\sqrt{12}a$ (red) and $\sqrt{19}a$ (green) superlattices in the real space (lower inset).

is demonstrated by the x -dependent evolution of (008) diffraction peak integrated intensities, where the growth of one end phase is at the expense of the other at the miscibility gap boundaries without continuous intermediate phase in between. As shown in Fig. 1 and Fig. 2, phase separation phenomenon is found to occur in two regions of $x \sim 0.76-0.82$ and $0.83-0.86$, where coexistence of two end phases grow at the expense of each other as indicated by the (008) X-ray diffraction peaks, while solid solution connects phases between miscibility gaps. Clearly the growth of 0.82 phase is at the expense of 0.76 phase for increasing x . Such coexisting pattern of two phases can only be observed in the narrow regions of $0.76-0.82$ and $0.83-0.86$, although O3-type secondary phase is commonly found for $x \gtrsim 0.85$ from melt growth.^{9,12} Pure $x \sim 0.86$ phase cannot be prepared using electrochemical technique, partly due to the fact that it becomes harder for Na to intercalate into the host structure of compressed c -axis.^{5,7} Enforcing more Na into the matrix electrochemically destroys its ordering as indicated by the broadened diffraction peaks that correspond to $x \gtrsim 0.86$ as shown in Fig. 2(a).

Fig. 3 shows synchrotron X-ray Laue diffraction results for $x = 0.801(5)$, where x sits in the middle of the miscibility gap of $0.76-0.82$. Although in-house x-ray results for x within $0.76-0.82$ range all display two-phase feature of the two end compounds only, the synchrotron X-ray Laue shows there are actually three coexist phases at room temperature. As shown in Fig. 3, we can clearly identify three twin sets of hexagonal superlattices that correspond to $\sqrt{19}a$, $\sqrt{13}a$ and $\sqrt{12}a$ in the real space, the latter two can be compared with the published single phase Laue patterns of $x = 0.71$ ($\sqrt{12}a$) and 0.84 ($\sqrt{13}a$).^{7,13} The newly found $\sqrt{19}a$ superlattice must be

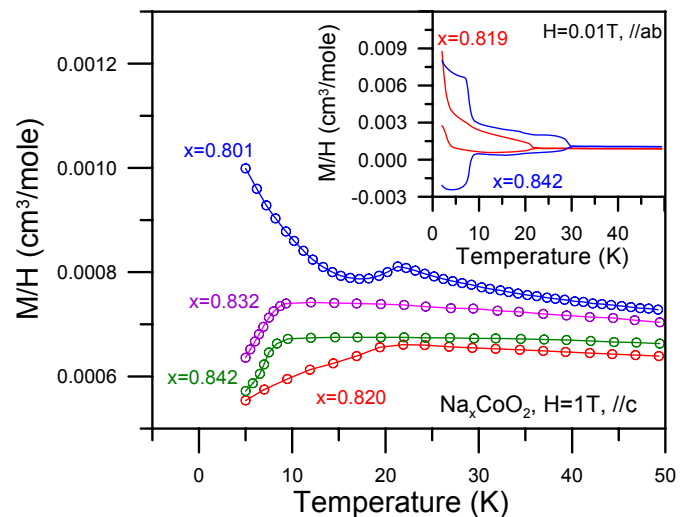


FIG. 4: (color online) Magnetic susceptibility measurement results for $x > 0.80$ under applied field of 1 Tesla and 0.01 Tesla (inset) along the c - and ab -directions respectively. All measurements were performed after being zero-field-cooled from room temperature through 200K with cooling rate of 2 K/min. A-type AF ordering is indicated by the cusp of c -axis susceptibility χ_c and the onsets of low field hysteresis shown in the inset.

due to Na ordering for $x \sim 0.76$ and has been verified by single phase sample, where more Na vacancies are introduced and a larger superlattice becomes necessary to accommodate larger multi-vacancy clusters. In fact it requires 4.5 vacancies per each superlattice of size $\sqrt{19}a$ to account for stoichiometry of $x \sim 0.76$, i.e. $x = 1 - \frac{4.5}{19} = 0.763$ that is composed of quadri- and penta-vacancy clusters in adjacent layers for γ - Na_xCoO_2 .^{7,13} A detailed analysis for $x \sim 0.76$ sample will be presented elsewhere. By treating this layered material to be a pseudo-binary system composed of Na and CoO_2 , the triple coexisting superlattices at constant temperature and pressure does not violate the phase rule, in fact it has reached the allowed maximum number of three. Considering dominant domains are from $x \sim 0.82$ ($\sqrt{13}a$ with di-vacancy clusters) and $x \sim 0.76$ ($\sqrt{19}a$ with quadri/penta-vacancy clusters), it's reasonable to have a buffered zone at the domain boundary which is built with tri/quadri-vacancy clusters of $\sqrt{12}a$ superlattice.

Most of the magnetic susceptibility measurements for Na_xCoO_2 with $x \gtrsim 0.75$ before show A-type AF signature near 22K, i.e., the cusp of χ_c under high field. Although crude magnetic phase mappings in this range before suggest that T_N varies between 22-27K,^{3,14} Schulze *et al.* recently found an additional 8K phase for $x \sim 0.80$ and 0.85 , which can be obtained only after a slow cooling process.¹⁰ With carefully tuned single crystals in the narrow range of $0.82-0.86$, we are able to re-visit the magnetic phase diagram and untangle the mystery of T_N variation. Magnetic susceptibility measurement results

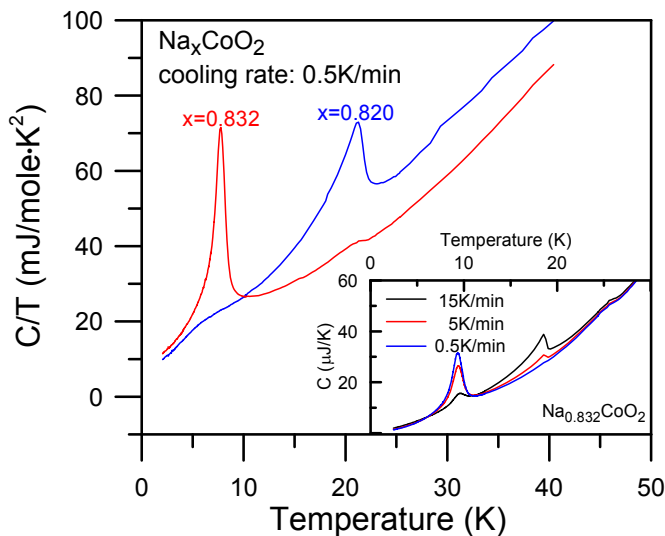


FIG. 5: (color online) Specific heat measurement results for $x = 0.820(3)$ and $0.832(2)$ obtained from slowest cooling rate of 0.5 K/min . The inset shows $x=0.832(2)$ has a strong cooling rate dependence, where 8 K phase grows at the expense of 16 K phase as cooling rate reduces from 15 to 0.5 K/min .

are shown in Fig. 4, all measurements were done after a slow cooling rate of 2 K/min . We find that T_N does not change with x monotonously and continuously, instead, the four phases at the two miscibility gap boundaries shown in Figs. 1 and 4 are responsible for the different characteristic T_N 's, where $x \sim 0.76$ shows Curie-Weiss behavior down to 5 K (not shown). The onsets of A-AF transitions are indicated by the cusp of χ_c under high field, which occur at $T_{N1}=22 \text{ K}$, $T_{N2}=8 \text{ K}$ and $T_{N3}=29 \text{ K}$ for $x = 0.820, 0.833$ and 0.859 respectively, while $0.801(5)$ and $0.842(5)$ data reflect their mixed phase nature, i.e., superposition of contributions from the end members of $0.76\text{-}0.82$ and $0.83\text{-}0.86$ miscibility gaps respectively. There is ZFC/FC irreversibility found below T_N for both χ_c and χ_{ab} at low field, although stronger FM saturation moments are seen along the ab -direction. Such A-AF ordering has been verified by the neutron scattering for $\text{Na}_{0.82}\text{CoO}_2$,⁴ where strong field dependence of magnetization below $T_N \sim 22 \text{ K}$ has been confirmed to be metamagnetic.¹⁵ Current low field measurement is in agreement with that reported for $x \sim 0.85$,¹⁰ although our data indicate that the 8 K phase is coming from the phase of x closer to 0.833 , while a more stable phase of 22 K is from x closer to 0.820 .

We find that the different onsets of A-AF transition between $x = 0.820(3)$ and $0.832(2)$ are clearly demonstrated by the cooling rate dependence of T_N as revealed by the specific heat data shown in Fig. 5, where 22 K transition for $x=0.820(3)$ is independent of cooling rate, while fast cooling rate moves T_N discretely from 8 K to 16 K for $x=0.832(2)$. 16 K phase occurs in $x=0.832(2)$ when a fast cooling is applied, while it decreases at the expense of

8 K phase generation under decreasing cooling rate, although the existence of minor 22 K is difficult to avoid completely for samples near the phase separated boundary. The ratio of the minor 22 K phase to the major 8 K phase in the present $x=0.833$ sample can be estimated to be 3.6% from the entropy change of the small anomaly at 22 K for $\text{Na}_{0.833}\text{CoO}_2$. Sodium ion diffusion is active at room temperature for high x samples,⁵ but it freezes below $\sim 200 \text{ K}$ as indicated by the sharp increase of $1/T_1$ for ^{23}Na due to Na motion.¹⁶ Sample of $x=0.832(2)$ must be cooled through the temperature range of $300\text{-}200 \text{ K}$ with a rate slower than 10 K/min in order to reach the magnetic ground state that corresponds to 8 K magnetic ordering.

The entropy associated with the 22 K transition in $\text{Na}_{0.820}\text{CoO}_2$ and the 8 K transition in $\text{Na}_{0.833}\text{CoO}_2$ are estimated to be $\Delta S \sim 170 \text{ mJ/mol K}$ and $\Delta S \sim 200 \text{ mJ/mol K}$, respectively. Taking the surface value of estimated ΔS and the transition width character, these results indicate that the magnetic moments order better in $\text{Na}_{0.833}\text{CoO}_2$ than in $\text{Na}_{0.820}\text{CoO}_2$. The relatively poor ordering of stage-2 for $x=0.820$ ($T_{N1}=22 \text{ K}$) than that of stage-5 $x=0.833$ ($T_{N2}=8 \text{ K}$) is interestingly in agreement with the alternating T-Q stacking requirement as described by the $x=0.71$ superstructure model before,^{7,13} i.e., tri-vacancy is not favorable in the even-layer within $P6_3/mmc$ symmetry and there must exist mixing stages of 1 and 3 for $x=0.820$. The ΔS value for $x=0.833$ is more than 10 times larger than that reported in Ref. [10], which suggests a nearly single 8 K phase in the present sample. On the other hand, these measured ΔS values are only about 20% of the entropy estimated from the complete ordering of fully localized spin- $1/2$ Co^{4+} ions. This discrepancy might indicate the failure of the simple ionic $\text{Co}^{3+}\text{-Co}^{4+}$ picture.

Since all samples with $x \gtrsim 0.82$ show identical superlattice size of $\sqrt{13}a$, the subtle difference for $x \sim 0.82$ and 0.83 must be related to the Na rearrangement generated by the additionally introduced Na defect that causes deviation from the ideal di-vacancy constructed $0.846=11/13$ of $\sqrt{13}a \times \sqrt{13}a \times 3c$ superstructure.^{7,13} But what kind of mechanism is responsible for these discrete T_N 's of Δx only $1\text{-}3\%$ apart? The secret lies in the stack ordering of 2 D hexagonal superlattices. From our previous studies on the structure of 0.71 and 0.84 ,^{7,13} the ideal superlattice has a $3c$ periodicity. The $3c$ periodicity for $x=0.820$ is once again confirmed by electron diffraction patterns on single domain crystals as shown in Fig. 6. Although $[001]_p$ diffraction pattern cannot tell the periodicity along c -direction, perfect indexing for diffraction patterns with transmitted beam along primitive $[101]_p$ and $[201]_p$ can only be achieved with the help of $3c$ periodicity assignment. When one and two more Na defects per $3c$ unit (i.e., six layers of Na) are introduced into the perfectly ordered original $0.846 = 11/13$ superstructure,⁷ two additional stoichiometries of $0.833 = 0.846 - \frac{1}{6} \times \frac{1}{13}$ and $0.820 = 0.846 - \frac{2}{6} \times \frac{1}{13}$ can be introduced, as verified by our X-ray and magnetic measurement results shown above. When magnetic ordering occurs, spins from itiner-

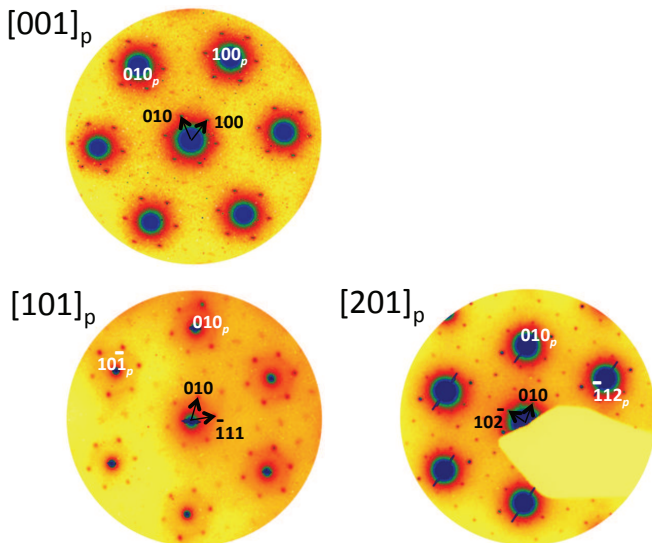


FIG. 6: (color online) Electron diffraction patterns of single domain $\text{Na}_{0.820}\text{CoO}_2$ for transmitted e-beam along $[001]_p$, $[101]_p$, and $[201]_p$ projections (p, denoting the primitive lattice). The superlattice spots surrounding the intense primitive cell reflections in the ab-plane projection, $[001]_p$, indicate the superlattice ordering of $\sqrt{13}\text{a} \times \sqrt{13}\text{a}$ without c-axis information. In the azimuthal projections of $[101]_p$ and $[201]_p$, the superlattice reflections suggests $3c$ ordering, i.e. can only be indexed correctly with $\sqrt{13}\text{a} \times \sqrt{13}\text{a} \times 3c$ superlattice.

ant electron or localized electrons near Co ions are certain to be affected by the rearrangement of Na multi-vacancy clusters in the nearby layers. In fact the in-plane inter-vacancy cluster distance $\sqrt{13}\text{a}$ is nearly twice the inter CoO_2 distance. Since every one extra Na vacancy introduced into the ideal $3c$ unit would convert the original layer of di-vacancy formed 2D superstructure into tri-vacancy, we can thus simplify the stacking problem into stack ordering between the di-vacancy (D) and tri-vacancy (T) layers along the c-direction. We propose a new staging model as shown in Fig. 1 to explain such stack ordering, which shows strong resemblance to the staging phenomenon often observed in the 2D intercalated graphite compounds.¹¹ The $x=0.833$ phase which has only one Na defect introduced could have a stage-5 construction, while $x=0.820$ phase of two Na defects per $3c$ unit must have a stage-2 construction, i.e., there are five and two D-layers sandwiched in between T-layers.

We can now use the staging picture to interpret the variety of magnetic ordering temperatures observed in the range $0.82 \lesssim x \lesssim 0.86$. As discussed previously,⁷ the di-vacancy may localize a carrier on the adjacent Co layer, leaving a low density hole gas of density $\frac{1}{13}$, which is unstable to Stoner ferromagnetism. This may be the

origin of the ferromagnetic layers which then order antiferromagnetically between layers to form the A type AF ordering. Here we suggest that the driving force for interlayer coupling may lie in the T-layer. The tri-vacancy has one extra negative charge which lowers the tunneling barrier between the localized holes on the adjacent layers and enhances the antiferromagnetic spin correlation between them. Thus the T-layer may form the nucleation layers to drive the three dimensional AF order. This picture explains why T_{N1} is 22K for $x=0.820$ vs. T_{N2} is 8K for $x=0.833$ where the spacing between T-layers is much larger. Upon rapid cooling, some stage 4 and stage 6 states may form. The stage 4 meta-stable phase may be responsible for the intermediate T_N of 16K. The hysteretic behavior observed below T_N (see Fig. 4) could also be explained by either the in-plane FM domain effect or by uncanceled A-type AF moments along the c-axis as a result of mixed staging. The phase separation observed near 0.83-0.86 can also be explained using the same stage model. Since $0.859=0.846+\frac{1}{6} \times \frac{1}{13}$, i.e., one more Na ion (not vacancy) is introduced into the original ideal $x=0.846$ phase of $\sqrt{13}\text{a} \times \sqrt{13}\text{a} \times 3c$ superstructure, the di-vacancy is converted to a mono-vacancy (M) forming a stage 5 stacking. The hole density on either side of the M-layer is now reduced by $\frac{1}{2} \times \frac{1}{13}$ and we may expect an even strong tendency toward Stoner ferromagnetism. The higher transition temperature of the Co layers adjacent to the M-layer may explain the higher $T_{N3} = 29\text{K}$ for $x=0.859$.

IV. CONCLUSIONS

In conclusion, we have revised Na_xCoO_2 phase diagram in the range of 0.71-0.86 using electrochemically fine tuned single crystal samples. The puzzling and inconsistent measurement results in this range before have been clarified and interpreted as a result of phase separation and staging phenomena. A direct link between the high temperature Na ion (vacancy) ordering and the low temperature magnetic properties have been established. The highly correlated ion, magnetic and charge orderings in layered Na_xCoO_2 can provide invaluable information to the study of strongly correlated electron low dimensional system which has itinerant electrons on a triangular lattice.

Acknowledgment

FCC acknowledges the support from National Science Council of Taiwan under project number NSC 97-3114-M-002. PAL acknowledges support by the DOE grant number DE-FG02-03ER46076.

* Electronic address: fchou@ntu.edu.tw

¹ M. L. Foo, Y. Wang, S. Watauchi, H. W. Zandbergen,

- T. He, R. J. Cava, and N. P. Ong, *Phys. Rev. Lett.* **92**, 247001 (2004).
- ² J. Wooldridge, D. M. Paul, G. Balakrishnan, and M. R. Lees, *J. Phys.: Condens. Matter* **17**, 707 (2005).
- ³ P. Mendels, D. Bono, J. Bobroff, G. Collin, D. Colson, N. Blanchard, H. Alloul, I. Mukhamedshin, F. Bert, A. Amato, et al., *Phys. Rev. Lett.* **94**, 136403 (2005).
- ⁴ S. P. Bayrakci, I. Mirebeau, P. Bourges, Y. Sidis, M. Enderle, J. Mesot, D. P. Chen, C. T. Lin, and B. Keimer, *Phys. Rev. Lett.* **94**, 157205 (2005).
- ⁵ G. J. Shu, A. Prodi, S. Y. Chu, Y. S. Lee, H. S. Sheu, and F. C. Chou, *Phys. Rev. B* **76**, 184115 (2007).
- ⁶ M. Roger, D. J. P. Morris, D. A. Tennant, M. J. Gutmann, J. P. Goff, J.-U. Hoffmann, R. Feyerherm, E. Dudzik, D. Prabhakaran, A. T. Boothroyd, et al., *Nature* **445**, 631 (2007).
- ⁷ F. C. Chou, M. W. Chu, G. J. Shu, F. T. Huang, W. W. Pai, H. S. Sheu, and P. A. Lee, *Phys. Rev. Lett.* **101**, 127404 (2008).
- ⁸ L. Balicas, Y. J. Jo, G. J. Shu, F. C. Chou, and P. A. Lee, *Phys. Rev. Lett.* **100**, 126405 (2008).
- ⁹ M. Lee, L. Viciu, L. Li, Y. Wang, M. L. Foo, S. Watauchi, R. A. P. Jr., R. J. Cava, and N. P. Ong, *Nature Materials* **5**, 537 (2006).
- ¹⁰ T. F. Schulze, P. S. Hafliger, C. Niedermayer, K. Mattenberger, S. Bubenhofer, and B. Batlogg, *Phys. Rev. Lett.* **100**, 026407 (2008).
- ¹¹ M. S. Dresselhaus and G. Dresselhaus, *Adv. Phys.* **51**, 1 (2002).
- ¹² G. J. Shu and F. C. Chou, *Phys. Rev. B* **78**, 052101 (2008).
- ¹³ F.-T. Huang, M.-W. Chu, G. J. Shu, H. S. Sheu, C. H. Chen, L.-K. Liu, P. A. Lee, and F. C. Chou, *Phys. Rev. B*, **79**, 014413 (2009).
- ¹⁴ J. Sugiyama, J. H. Brewer, E. J. Ansaldo, H. Itahara, T. Tani, M. Mikami, Y. Mori, T. Sasaki, S. Hebert, and A. Maignan, *Phys. Rev. Lett.* **92**, 017602 (2004).
- ¹⁵ J. L. Luo, N. L. Wang, G. T. Liu, D. Wu, X. N. Jing, F. Hu, and T. Xiang, *Phys. Rev. Lett.* **93**, 187203 (2004).
- ¹⁶ K. Yoshimura, H. Ohta, C. Michioka, and Y. Itoh, *J. Magn. Mater.* **310**, 693 (2007).